COBEM 2023 27TH INTERNATIONAL CONGRESS OF MECHANICAL ENGENEERING

ABCM Brazilian Society of Mechanical Sciences and Engineering
27th ABCM International Congress of Mechanical Engineering
December 04-08, 2023, Florianópolis-SC, Brazil

COB-2023-1451
RELIABILITY ESTIMATION OF CRACK PROPAGATION IN A ROTATING MACHINE SHAFT USING BAYESIAN DEEP LEARNING

Matheus de Moraes[1]
Douglas Massakatsu Kohatsu[1]
João Paulo Dias[2]
Hélio Fiori de Castro[1]
[1]School of Mechanical Engineering, State University of Campinas, 200 Mendeleyev Street, 13083-860, Campinas, São Paulo, Brazil
m263136@dac.unicamp.br
doug.kohatsu@gmail.com
hfc@unicamp.br
[2]Dept. of Civil and Mechanical Engineering, Shippensburg University of Pennsylvania, 1871 Old Main Drive, 17257, Shippensburg, Pennsylvania, United States
JPDias@ship.edu

Abstract. *Rotating machines are essential in several engineering applications. For this reason, unexpected overloads can cause damage to their components, and the damage can cause accidents and losses of revenue. Furthermore, computational modeling and deep learning techniques are transforming industrial activities and supporting the decision-making of manufacturing and maintenance tasks. This work presents a condition monitoring technique based on Bayesian neural networks, which includes uncertainties quantification, to estimate crack length in a rotating shaft, then estimate the reliability using First Order Reliability Method (FORM) and Second Order Reliability Method (SORM). Several simulations of a shaft operating with different crack lengths were performed. A Bayesian Neural Network were employed to estimate the crack length. The crack was propagated using Paris Law, and then the reliability was assessed. By examining the constructed BNN model, we were able to observe and assess the level of uncertainty in the predictions. This provides us with additional insights into the failure data of equipment, ultimately aiding in the monitoring of rotating machine condition and crack propagation using the Paris Law. Furthermore, it enables us to evaluate reliability through the use of FORM and FORM and the results were satisfatory comparing with the Monte Carlo method.*

Keywords: *rotating machines, condition monitoring, Bayesian neural networks, SORM and FORM, remaining useful life*

1. INTRODUCTION

Rotating machines play a fundamental role in meeting the demands of modern society. They are employed in tasks within the manufacturing industry (Iliyas Ahmad *et al.*, 2020), in transportation (Sun *et al.*, 2021), in wastewater treatment (Ma *et al.*, 2020), in power conversion and generation (Du *et al.*, 2020), and in other applications. On the other hand, defects in rotating machinery can generate immeasurable damage. For example, the economic losses associated with maintenance in Brazil are approximately 4% of the gross sales of industries (Oliveira, 2013). However, the costs are not only in finances but socio-environmental, such as accidents and waste of revenues. Moreover, the fourth industrial revolution has been shaping up since the last decade. This new conjuncture incorporates Artificial Intelligence (AI), the Internet of Things (IoT), cloud computing, and digital twins into traditional activities such as manufacturing and maintenance. The impacts of this revolution are causing a significant increase in the condition monitoring routines of rotating machines and, in this way, helping decision-making in order to reduce errors and costs.

Many works in the literature employ artificial intelligence and uncertainty quantification for rotating machinery condition monitoring, and it is possible to affirm that these kinds of application of data science techniques are the scientific vanguard employed in rotating machinery condition monitoring (Liu *et al.*, 2018). The work of Alves *et al.* (2020) presents a study involving the development of a finite element model and simulation of ovalization failure in the hydrodynamic bearings of a rotor and performing fault diagnosis for different severity levels using convolutional neural networks (CNN). Wang *et al.* (2020) elaborate on a remaining useful life (RUL) prediction technique using experimental data from accelerated life tests with rolling bearings, using Bayesian convolutional neural networks (BCNN) to estimate the degradation state of the equipment. The results proved effective for machine prognosis. The paper by Wang *et al.* (2021) presents the comparison between Bayesian neural networks (BNN) and Bayesian logistic regression (BLR) techniques. They tested both techniques experimentally for performing condition monitoring of a naval internal combustion engine, and the results were superior to often used methodologies. The academic paper by Peng *et al.* (2020) presented two different architectures for Bayesian Neural Networks (BNN) aiming to estimate the RUL. The experimental data are from tests with Turbofan

engines tested until the bearing failure. After that, the input data are complex time-frequency features in one of the networks and time series in the other. As a result, the RUL probability density function is presented and compared with the lifetime in an experiment. Both network architectures show the RUL estimation with high precision and quantified levels of uncertainty. The study by Kitai *et al.* (2021) proposes a new RUL estimation approach that uses CNN and hierarchical Bayesian regression (HBR). Then, the input data preprocessing of the CNN generated spectrograms is the methodology's novelty. The results show a significant increment in the accuracy of the RUL prediction. They used these images as input data in two parallel network architectures: the first with data history for different degradation states, and in the other CNN, the input is only a spectrogram image of the last observation of the degradation state. Thus, both predictions are compared and applied in HBR, which can estimate the uncertainties of the RUL prediction. de Moraes *et al.* (2021) present the diagnosis of ball-bearing failures by transforming time signatures into vibration images. These data feed a convolutional BNN, and during the tests, the work shows diagnoses for different types of damages and different severities and performs the uncertainties quantification of these diagnoses. Barbosa and Rade (2022) studied the reliability analysis of rotor-bearing systems of Kriging surrogate models and the First-Order Reliability Method (FORM). The results from the comparison between several combinations of classical techniques show that the Kriging/FORM strategy decreases computation costs while maintaining acceptable precision in assessing reliability.

Although all these contributions in the literature have been made so far, it is possible to note the lack of applications of machine learning algorithms combined with the uncertainties quantification for shaft crack diagnosis and reliability. Thus, we have pursued the answer to the following research question: can Bayesian neural networks be used to quantify the uncertainty on the estimation of the crack length in a shaft and support an estimative of reliability? The specific objectives of this research are: (i) a finite element model capable of simulating vibration signals in the rotating shaft condition operating with different crack lengths; (ii) to develop and train a Bayesian Neural Network (BNN) algorithm to quantify uncertainties on crack length predictions; (iii) to predict the crack propagation parameters using Paris Law and estimate reliability using First Order Reliability Method (FORM) and Second Order Reliability Method (SORM).

Following this Section 1, this work is organized in Methodology (Section 2.), in which it is presented the way the finite element model of the rotor under analysis was developed, as well as the techniques used to develop the BNN model. Then, the main results are presented and discussed in Section 3. Finally, the main conclusions obtained from the work are presented in Section 4..

2. METHODOLOGY

2.1 Mathematical Modeling of the rotor

The Finite Element Method (FEM) is often used to model continuous rotating elements. It allows for the coupling between translational and rotational movements. The rotor under analysis is discretized using 11 Timoshenko beam elements, with each element consisting of 4 degrees of freedom (DOFs) per node - two translational DOFs and two rotational DOFs. Figure 1 illustrates a schematic diagram of the finite element model of the rotor, highlighting the 6 nodes that couple 5 Timoshenko beams, the crack in the fifth element, as well as the positions of the disc at node number 3 and the bearings at nodes 1 and 6.

Additionally, the Lagrange formulation is employed to incorporate a rigid disc element, enabling the derivation of the equations of motion for the mechanical system, as follows:

$$\mathbf{M}\ddot{\mathbf{q}}(\mathbf{t}) + (\mathbf{C} + \Omega\mathbf{G})\dot{\mathbf{q}}(t) + \mathbf{K}\mathbf{q}(t) = \mathbf{f}(t), \tag{1}$$

in which, $\mathbf{M}$ is the global mass matrix, $\mathbf{K}$ is the global stiffness matrix, $\mathbf{C} = \alpha\mathbf{M} + \beta\mathbf{K}$ is the global stiffness is the global damping matrix, $\mathbf{G}$ is the global gyroscopic, Ω is the shaft's angular velocity (spin), $\mathbf{f}(t)$ is the vector of the external forces applied to the rotor and $\mathbf{q}(t)$ is the vector of generalized coordinates, α e β are proportionality factors.

2.2 Modeling the crack in the shaft

The crack model is the same as presented in the literature (Garoli and de Castro, 2020), and the study of cracking in shafts is relevant due to the fatigue phenomenon. The area moments of inertia in the directions of the centroids ($\bar{y}$ and $\bar{z}$) of the shaft element are constant, even when operating in rotation, and can be described in an asymmetric shaft. Furthermore, there is a possibility that the area moments of inertia of the inertial referential coordinates ($\bar{Y}$ and $\bar{Z}$) can be developed as area moments of inertia of the rotational referential coordinates $I_{\bar{y}}$ and $I_{\bar{z}}$ in a form:

$$\begin{aligned} I_{\bar{Y}}(t) &= \tfrac{I_{\bar{y}}+I_{\bar{z}}}{2} + \tfrac{I_{\bar{y}}+I_{\bar{z}}}{2}\cos(2\omega t) + I_{\bar{y}\bar{z}}\sin(2\omega t) \\ I_{\bar{Y}}(t) &= \tfrac{I_{\bar{y}}+I_{\bar{z}}}{2} - \tfrac{I_{\bar{y}}+I_{\bar{z}}}{2}\cos(2\omega t) - I_{\bar{y}\bar{z}}\sin(2\omega t) \\ I_{\bar{Z}\bar{Y}}(t) &= -\tfrac{I_{\bar{y}}-I_{\bar{z}}}{2}\sin(2\omega t) + I_{\bar{y}\bar{z}}\cos(2\omega t), \end{aligned} \tag{2}$$

where, $I_{\bar{y}} = I_y - A_{ce}e$, $I_{\bar{z}} = I_z$, I_y e I_z are area moment of inertia in the rotational reference frame, A_{ce} is the area

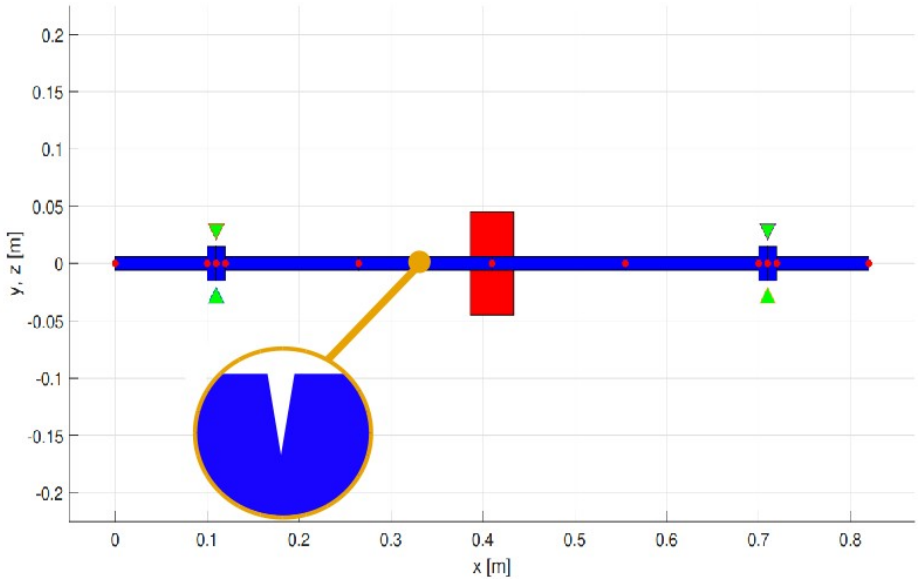

Figure 1: Diagram of the rotor used in simulations.

of cross-section of the cracked shaft element, and e is the centroid's position in the vertical direction z. $I_{\bar{y}\bar{z}}$ is null once the axis direction z has a symmetric split in the cross-section of the cracked element. The calculation of the cross-section with the crack A_{ce}, the centroid's position e and the area inertia moments in the rotating frame I_y e I_z, as follows:

$$\begin{aligned} A_{ce} &= R^2[\pi - \cos^{-1}(1-\mu) + (1-\mu)\sqrt{\mu(2-mu)}] \\ e &= \tfrac{2R^3}{3A_{ce}}[\mu(2-\mu)]^{\frac{3}{2}}, \end{aligned} \tag{3}$$

$$\begin{aligned} I_y &= \tfrac{\pi R^4}{4} + \tfrac{R^4}{4}[(1-\mu)(2\mu^2-4\mu-1)\sqrt{\mu(2-\mu)} + \sin^{-1}(1-\mu)] \\ I_z &= \tfrac{\pi R^4}{4} + \tfrac{R^4}{12}[(1-\mu)(2\mu^2-4\mu-3)\sqrt{\mu(2-mu)} + 3\sin^{-1}\sqrt{\mu(2-\mu)}], \end{aligned} \tag{4}$$

in which, $\mu = \frac{h_t}{R}$ is the adimentional crack depth, h_t is the crack depth and R the radius of cross-section of the shaft element. We have the stiffness matrix of the cracked element in the rotational reference frame, given by:

$$\mathbf{K}_{cr} = \frac{E}{L^3}\begin{bmatrix} 12I_{\bar{y}} & & & & & & & \\ 0 & 12I_{\bar{z}} & & & & & & \\ 0 & -6LI_{\bar{z}} & 4L^2I_{\bar{z}} & & & \text{sym.} & & \\ 6LI_{\bar{y}} & 0 & 0 & 4L^2I_{\bar{y}} & & & & \\ -12LI_{\bar{y}} & 0 & 0 & -6LI_{\bar{y}} & 12I_{\bar{y}} & & & \\ 0 & -12LI_{\bar{z}} & 6LI_{\bar{z}} & 0 & 0 & 12I_{\bar{z}} & & \\ 0 & -6LI_{\bar{z}} & 2L^2I_{\bar{z}} & 0 & 0 & 6LI_{\bar{z}} & 4L^2I_{\bar{z}} & \\ 6LI_{\bar{y}} & 0 & 0 & 2L^2I_{\bar{y}} & -6LI_{\bar{y}} & 0 & 0 & 4L^2I_{\bar{y}} \end{bmatrix}, \tag{5}$$

where, E is the shaft's material Young's modulus and L is the length of the shaft element. The projection of the matrix in the inertial reference frame is given by:

$$\mathbf{K}_{c_f} = \mathbf{K}_a + \mathbf{K}_b, \tag{6}$$

being,

$$\mathbf{K}_a = \frac{E}{L^3}\begin{bmatrix} 12I_{\bar{Y}} & & & & & & & \\ 0 & 12I_{\bar{Z}} & & & & \text{sym.} & & \\ 0 & -6LI_{\bar{Z}} & 4L^2I_{\bar{Z}} & & & & & \\ 6LI_{\bar{Y}} & 0 & 0 & 4L^2I_{\bar{Y}} & & & & \\ -12LI_{\bar{Y}} & 0 & 0 & -6LI_{\bar{Y}} & 12I_{\bar{Y}} & & & \\ 0 & -12LI_{\bar{Z}} & 6LI_{\bar{Z}} & 0 & 0 & 12I_{\bar{Z}} & & \\ 0 & -6LI_{\bar{Z}} & 2L^2I_{\bar{Z}} & 0 & 0 & 6LI_{\bar{Z}} & 4L^2I_{\bar{Z}} & \\ 6LI_{\bar{Y}} & 0 & 0 & 2L^2I_{\bar{Y}} & -6LI_{\bar{Y}} & 0 & 0 & 4L^2I_{\bar{Y}} \end{bmatrix}, \tag{7}$$

and,

$$\mathbf{K}_b = \frac{E}{L^3}\begin{bmatrix} 0 & & & & & & & \\ -12I_{\bar{Z}\bar{Y}} & 0 & & & & & & \\ 6LI_{\bar{Z}\bar{Y}} & 0 & 0 & & \text{sym.} & & & \\ 0 & -6LI_{\bar{Z}\bar{Y}} & 4L^2I_{\bar{Z}\bar{Y}} & 0 & & & & \\ 0 & 12LI_{\bar{Z}\bar{Y}} & -6I_{\bar{Z}\bar{Y}} & 0 & 0 & & & \\ 12I_{\bar{Z}\bar{Y}} & 0 & 0 & 6LI_{\bar{Z}\bar{Y}} & -12I_{\bar{Z}\bar{Y}} & 0 & & \\ 6LI_{\bar{Z}\bar{Y}} & 0 & 0 & 2L^2I_{\bar{Z}\bar{Y}} & -6LI_{\bar{Z}\bar{Y}} & 0 & 0 & \\ 0 & -6LI_{\bar{Z}\bar{Y}} & 2L^2I_{\bar{Z}\bar{Y}} & 0 & 0 & 6LI_{\bar{Z}\bar{Y}} & 4L^2I_{\bar{Z}\bar{Y}} & 0 \end{bmatrix}, \tag{8}$$

the matrix $\mathbf{K}_{c_f}$ can be rewritten:

$$\mathbf{K}_{c_f} = \mathbf{K}_{c_0} + \mathbf{K}_{c_c}\cos(2\omega t) + \mathbf{K}_{c_s}\sin(2\omega t), \tag{9}$$

in which,

$$\mathbf{K}_{c_0} = \frac{E}{L^3}\begin{bmatrix} 12I_1 & & & & & & & \\ 0 & 12I_1 & & & & \text{sym.} & & \\ 0 & -6LI_1 & 4L^2I_1 & & & & & \\ 6LI_1 & 0 & 0 & 4L^2I_1 & & & & \\ -12LI_1 & 0 & 0 & -6LI_1 & 12I_1 & & & \\ 0 & -12LI_1 & 6LI_1 & 0 & 0 & 12I_1 & & \\ 0 & -6LI_1 & 2L^2I_1 & 0 & 0 & 6LI_1 & 4L^2I_1 & \\ 6LI_1 & 0 & 0 & 2L^2I_1 & -6LI_1 & 0 & 0 & 4L^2I_1 \end{bmatrix}, \tag{10}$$

$$\mathbf{K}_{c_c} = \frac{E}{L^3}\begin{bmatrix} 12I_2 & & & & & & & \\ 0 & 12I_2 & & & & \text{sym.} & & \\ 0 & -6LI_2 & 4L^2I_2 & & & & & \\ 6LI_2 & 0 & 0 & 4L^2I_2 & & & & \\ -12LI_2 & 0 & 0 & -6LI_2 & 12I_2 & & & \\ 0 & -12LI_2 & 6LI_2 & 0 & 0 & 12I_2 & & \\ 0 & -6LI_2 & 2L^2I_2 & 0 & 0 & 6LI_2 & 4L^2I_2 & \\ 6LI_2 & 0 & 0 & 2L^2I_2 & -6LI_2 & 0 & 0 & 4L^2I_2 \end{bmatrix}, \tag{11}$$

$$\mathbf{K}_b = \frac{E}{L^3}\begin{bmatrix} 0 & & & & & & & \\ -12I_2 & 0 & & & & & & \\ 6LI_2 & 0 & 0 & & \text{sym.} & & & \\ 0 & -6LI_2 & 4L^2I_2 & 0 & & & & \\ 0 & 12LI_2 & -6I_2 & 0 & 0 & & & \\ 12I_2 & 0 & 0 & 6LI_2 & -12I_2 & 0 & & \\ 6LI_2 & 0 & 0 & 2L^2I_2 & -6LI_2 & 0 & 0 & \\ 0 & -6LI_2 & 2L^2I_2 & 0 & 0 & 6LI_2 & 4L^2I_2 & 0 \end{bmatrix}, \tag{12}$$

with $I_1 = \frac{1}{2}(I_{\bar{y}} + I_{\bar{z}})$ and $I_2 = \frac{1}{2}(I_{\bar{y}} - I_{\bar{z}})$.

2.3 Equations of motion solution using harmonic balance method

The equations of motion solution and external loads are expressed as a Fourier series to an order of C_h:

$$\begin{array}{l} \mathbf{q} = \mathbf{q}_0 + \sum_{k=1}^{C_h} \mathbf{q}_{c_k} \cos(k\omega t) + \mathbf{q}_{s_k} \sin(k\omega t) \\ \mathbf{f} = \mathbf{f}_0 + \sum_{k=1}^{C_h} \mathbf{f}_{c_k} \cos(k\omega t) + \mathbf{f}_{s_k} \sin(k\omega t) \end{array}, \tag{13}$$

we have, the stiffness matrix rewritten:

$$\mathbf{K} = \mathbf{K}_0 + \sum_{k=1}^{C_h} \mathbf{K}_{c_k} \cos(k\omega t) + \mathbf{K}_{s_k} \sin(k\omega t). \tag{14}$$

The solution are obtained through the solution of the following system

$$\mathbf{HQ} = \mathbf{F}, \tag{15}$$

being,

$$\begin{array}{l} \mathbf{Q} = [\mathbf{q}_0\ \mathbf{q}_{c_1}\ \mathbf{q}_{s_1}\ \mathbf{q}_{c_2}\ \mathbf{q}_{s_2}\ \cdots\ \mathbf{q}_{c_{C_h}}\ \mathbf{q}_{s_{C_h}}]^T \\ \mathbf{F} = [\mathbf{f}_0\ \mathbf{f}_{c_1}\ \mathbf{f}_{s_1}\ \mathbf{f}_{c_2}\ \mathbf{f}_{s_2}\ \ldots\ \mathbf{f}_{c_{C_h}}\ \mathbf{f}_{s_{C_h}}]^T \end{array}$$

$$\mathbf{H} = \begin{bmatrix} K_0 & 0 & 0 & \frac{1}{2}K_{c_1} & \frac{1}{2}K_{s_1} & 0 & 0 & 0 & 0 & \ldots & 0 & 0 \\ 0 & U_1 + \frac{1}{2}K_{c_1} & U_1 + \frac{1}{2}K_{s_1} & 0 & 0 & \frac{1}{2}K_{c_1} & \frac{1}{2}K_{s_1} & 0 & 0 & \ldots & 0 & 0 \\ 0 & -U_1 + \frac{1}{2}K_{s_1} & U_1 + \frac{1}{2}K_{c_1} & 0 & 0 & -\frac{1}{2}K_{s_1} & \frac{1}{2}K_{c_1} & 0 & 0 & \ldots & \vdots & \vdots \\ K_{c_2} & 0 & 0 & U_2 & 2\omega C & 0 & 0 & \frac{1}{2}K_{c_2} & \frac{1}{2}K_{s_2} & \ddots & 0 & 0 \\ K_{s_2} & 0 & 0 & -2\omega C & U_2 & 0 & 0 & -\frac{1}{2}K_{s_2} & \frac{1}{2}K_{c_2} & \ddots & \frac{1}{2}K_{c_{C_h}} & \frac{1}{2}K_{s_{C_h}} \\ 0 & \frac{1}{2}K_{c_3} & \frac{1}{2}K_{s_3} & 0 & 0 & U_3 & 3\omega C & 0 & 0 & \ddots & -\frac{1}{2}K_{s_{C_h}} & \frac{1}{2}K_{c_{C_h}} \\ 0 & -\frac{1}{2}K_{s_3} & \frac{1}{2}K_{c_3} & 0 & 0 & -3\omega C & U_3 & 0 & 0 & \ddots & 0 & 0 \\ \vdots & \ddots & \ddots & \ddots & \ddots & \ddots & \ddots & \ddots & \ddots & \ddots & 0 & 0 \\ 0 & 0 & 0 & 0 & \ldots & 0 & \frac{1}{2}K_{c_{C_h}} & \frac{1}{2}K_{s_{C_h}} & 0 & 0 & U_{C_h} & -C_h\omega C \\ 0 & 0 & 0 & 0 & \ldots & 0 & -\frac{1}{2}K_{s_{C_h}} & \frac{1}{2}K_{c_{C_h}} & 0 & 0 & -C_h\omega C & U_{C_h} \end{bmatrix},$$

where, $U_k = K_0 - (k\omega)^2\mathbf{M}$. Thus, the calculation of the dynamic response of the rotating system and its harmonics solving the system $\mathbf{Q}$.

2.4 Bayesian Neural Networks

Bayesian neural networks (BNN) are a supervised machine learning algorithm that takes accounts for the effects of uncertainty. BNNs are composed of probabilistic layers with θ parameters, which differs from traditional artificial neural networks, whose model with deterministic parameters. The main idea of BNNs is to estimate the probability density function a *posteriori* of the θ parameters from a D data set and application of Bayes' Theorem::

$$p(\theta|D) = \frac{p(D|\theta)p(\theta)}{\int p(D|\theta')p(\theta')d\theta'}, \tag{16}$$

where, $p(\theta|D)$ is the posterior probability density function of the parameter θ, $p(D|\theta)$ is the likelihood function, $p(\theta)$ is the prior pdf of the θ and $\int p(D|\theta')p(\theta')d\theta'$ is a normalization constant.

Variational inference is the technique commonly used to approximate the posterior distribution by minimizing the Kullback-Leibler divergence $\mathbf{D_{KL}}$ among any distribution $q(\theta|\omega)$ that belongs to a family of distributions Q and the posterior distribution $p(\theta|D)$. This operation is equivalent to maximizing the *Evidence Lower Bound* (ELBO) function (Blundell *et al.*, 2015; San Martin *et al.*, 2019; Vega and Todd, 2020):

$$ELBO(q(\theta|\omega)) = \mathbb{E}_{q(\theta|\omega)}(\log p(\theta|D) - \mathbf{D_{KL}}(q(\theta|\omega)||p(\theta)), \tag{17}$$

where $\mathbb{E}_{q(\theta|\omega)}(\log p(\theta|D))$ is the expectation of the log-evidence and $p(\theta)$ is the prior pdf of the parameters set θ.

In this work, we used open-source libraries Tensorflow and Tensorflow probability (TFP) to build the BNN model. The configuration of weights and biases of the neurons in the network layers can perform variational inference, the variational layers. These layers allow the weights and biases to be adjusted in posterior distributions, incorporating statistical distributions into the model architecture. The model includes uncertainty in the neural network model by converting each weight from a point estimate (deterministic) to a probability distribution. The training step allows tuning the model parameters to obtain the parameters of these distributions.

The backpropagation Bayesian algorithm starts with a prior distribution definition over the parameters, which means belief about the θ parameters of the model given the lack of information of any D data set. The implementation of dense variational layers – layers in which all neurons receive information from all neurons of the previous layer and which admit the use of variational inference in the definition of weights and biases – consists of defining the prior and posterior distributions over the kernel and the *bias*. Then it is inserted into the layers via the posterior kernel function, which has parameters described by mean and standard deviation. The kernel matrix receives the posterior distribution. On the other hand, the definition of the arguments of a prior kernel function by a spherical Gaussian with zero mean and unit standard deviation. Finally, the network learns the posterior distribution of the parameters using variational inference, in other words, by optimizing $\mathbf{D_{KL}}$.

2.5 Discretized Paris Law for crack propagation

The Paris law, formulated by Paris and Erdogan (1963), is a mathematical model used to estimate the growth of crack size and to calculate the Remaining Useful Life (RUL) of a cracked part. This law expresses the relation between the stress intensity factor, the crack length, and the number of cycles. In this work, we use the discretized Paris Law (Endeshaw *et al.*, 2017) to estimate crack growth as we account for several cycles:

$$a_k = a_{k-1} + Q(\gamma(\sigma_{max} - \sigma_{min})\sqrt{\pi a_{k-1}})^n \Delta N \tag{18}$$

where, a_k is the estimated crack size after crack propagation, a_{k-1} is the actual crack size before propagation, Q and n are constants that vary according to the type of material used, γ is a dimensionless geometric factor, ΔN is the number of cycles that will occur for the crack to reach a_k size, and σ_{max} and σ_{min} are the maximum and minimum stresses, *i. e.*, the stress amplitude.

2.6 First order reliability method and second order reliability method

Assessing the structural reliability of the rotating system requires specific methods such as the Monte Carlo Method, the First Order Reliability Method (FORM), and the Second Order Reliability Method (SORM) to solve the reliability equation given by:

$$P_f = P\{g(X) < 0\} = \int_{g(X)<0} f_x(X)dX \tag{19}$$

where, $g(X)$ is the limit state, $f_x(X)$ is the set of probability density function (pdf).

The FORM finds the probability of failure, i.e., the reliability complement. To accomplish this, FORM solves the problem of equation 19 by approximating the limit state function by the first-order expansion of the Taylor series. In turn, SORM similar to FORM, it also finds the probability of failure, but unlike FORM, SORM approximates the limit state function by a second-order expansion of the Taylor series (Nannapaneni and Mahadevan, 2016; Kang *et al.*, 2016).

3. RESULTS AND DISCUSSION

3.1 Estimation of shaft crack length using BNN

To develop the Bayesian neural network (BNN) model for predicting the shaft crack size, we conducted simulations of the shaft operating with 2000 distinct normalized crack lengths and varying angular velocities Ω. The crack's localization is in the fifth element of the rotor (see Fig. 1), and it does not change for any simulation. From these simulations, we extracted six statistical parameters of the time signature: root mean square (RMS) value, kurtosis, asymmetry, peak value, minimum value, and the ratio between peak and RMS.

We constructed BNN with 12 layers, each containing 12 neurons, and this architecture exhibited the best performance among the tested configurations. The simulations using the finite element model (FEM) generated a dataset of 2000 samples, of which 1500 were used for training and 500 for testing. Figure 2 presents the loss function plotted against the number of epochs.

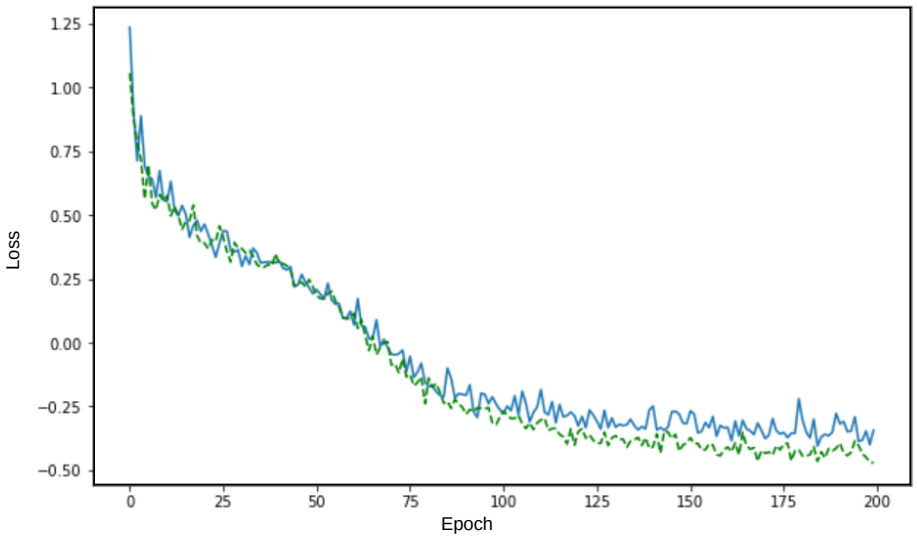

Figure 2: plot of the loss function *versus* the number of epochs

The graph of Figure 2 shows that the training and validation curves closely align, indicating the absence of overfitting. Furthermore, the loss function remains constant after 175 epochs, suggesting that no significant improvement in training occurs beyond this point.

Figure 3 presents the graph of 20 independent predictions performed by the BNN model. In Figure 3 we can notice the average prediction for 20 independent samples and the epistemic uncertainties associated with each prediction for a 95% confidence interval. We verified that the average value of the normalized crack length predictions obtained by the BNN model are close to the normalized crack length values obtained by the simulations, and although some points are distant, they are within the defined confidence interval, which indicates the degree of uncertainty of the presented data.

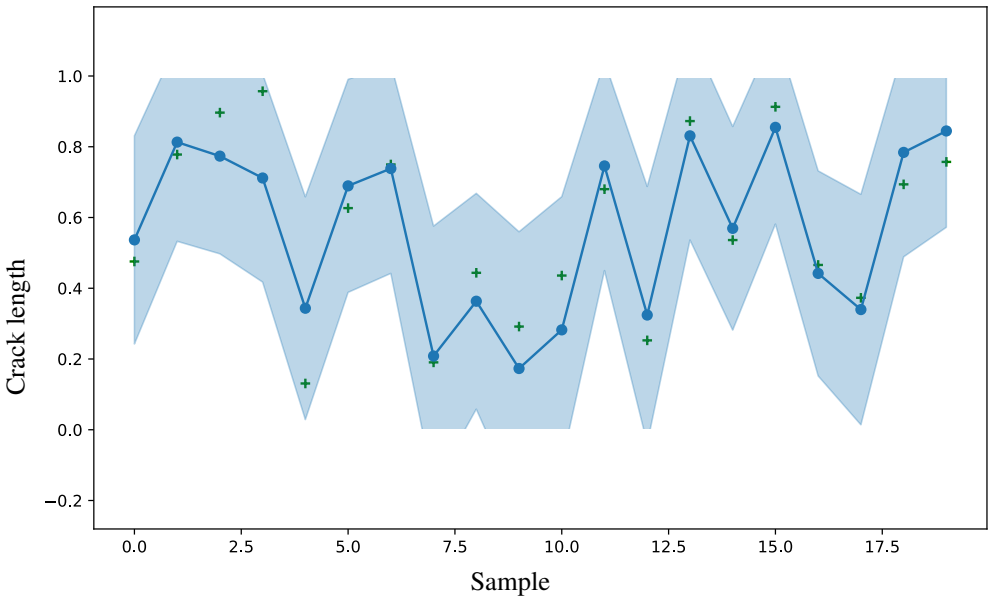

Figure 3: Plot of the predictions in blue (-.-), the values of the normalized crack length predicted by BNN and the geen dots (+) inditcate the test data. The shadowed area represents the 95% confidence interval of the predictions.

For further investigation of the prediction values, we plot histograms of 4 randomly obtained samples. Figure 4 shows these histograms.

From observing these histograms it is possible to see that the central tendency of the distributions are very close to the values of the tested crack lengths, and it is also possible to obtain the degree of uncertainty of the model predictions,

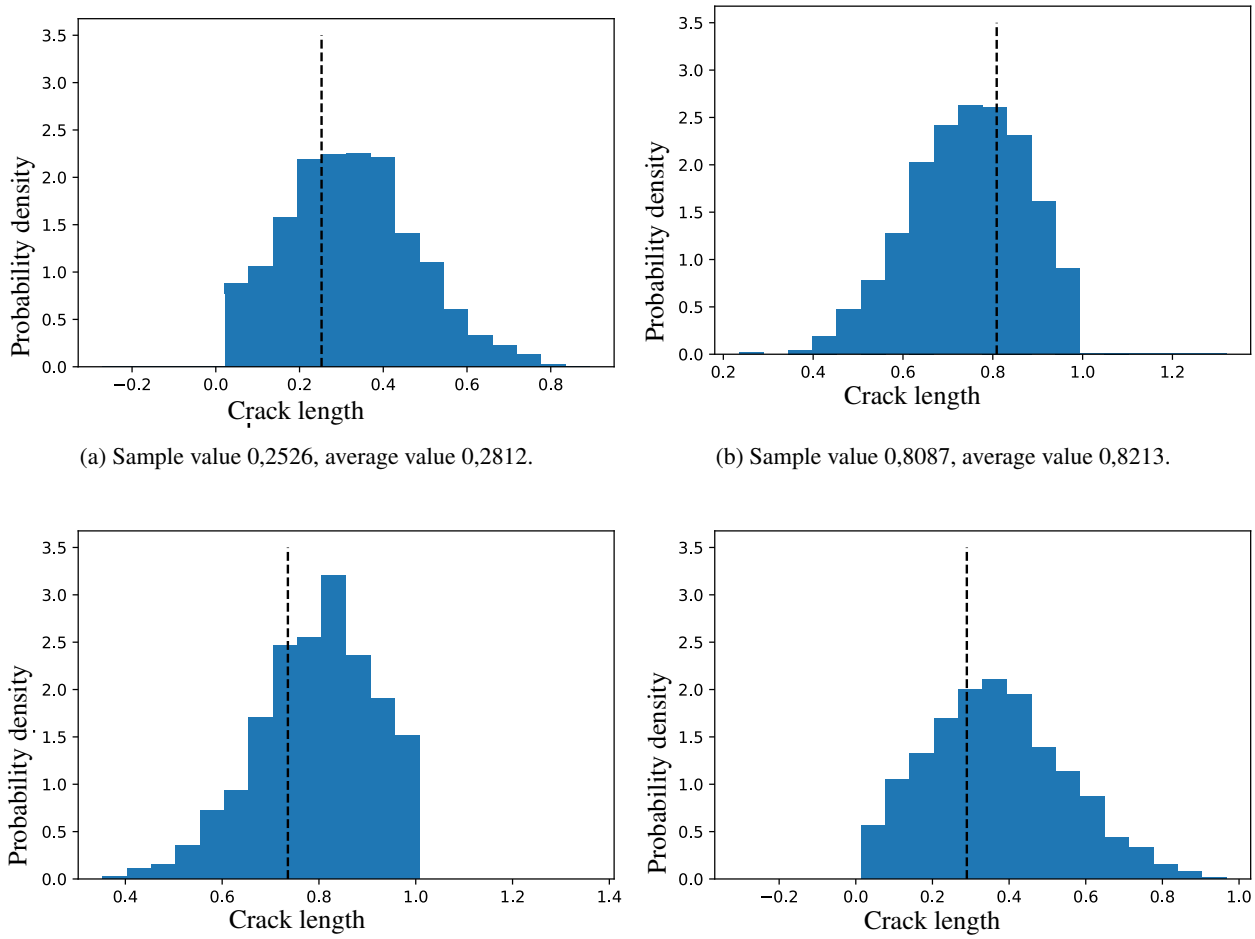

(a) Sample value 0,2526, average value 0,2812.

(b) Sample value 0,8087, average value 0,8213.

(c) Sample value 0,7358, average value 0,7641.

(d) Sample value 0,2897, average value 0,3492.

Figure 4: Histograms of normalized crack length, the vertical dashed line indicates the value of the sample.

which is important information in condition monitoring tasks. In addition, these normalized crack length distributions can be used to evaluate the reliability of the machine operating at a given time instant.

3.2 First order reliability method and second order reliability method.

To simulate the crack propagation using Paris law, we take the case in which the mean value of the normalized crack size is 0.2526 of the radius, and the standard deviation is 0.1492. In Figure 5, we have the graph of the propagation of the crack size, with its uncertainty propagation. We can notice that the uncertainty of the crack size grows with the increasing number of cycles. This behavior is as expected once the number of cycles increases there is less information regarding its behavior. Furthermore, according to the graph, even starting with a large crack size, which is 25% of the shaft radius, it took 7.8×10^4 cycles for the reliability to start decreasing. We can affirm that some samples achieves the catastrophic failure in this number of cycles.

Figure 6 shows the plot of reliability variation with increasing number of cycles for the rotating shaft. In Figure 6, we have a decrease in reliability during the crack propagation and it is abrupt when the achieves 7.8×10^4 cycles. It reaches near-zero quickly, needing only about 3×10^4 cycles.

4. CONCLUSIONS

The main conclusions of the work are:

- the implementation of a finite element model operating with a crack allowed the simulation of several different lengths of failures in the rotating machine;
- the Bayesian neural network model construction, training with simulated data, evaluating its performance, and

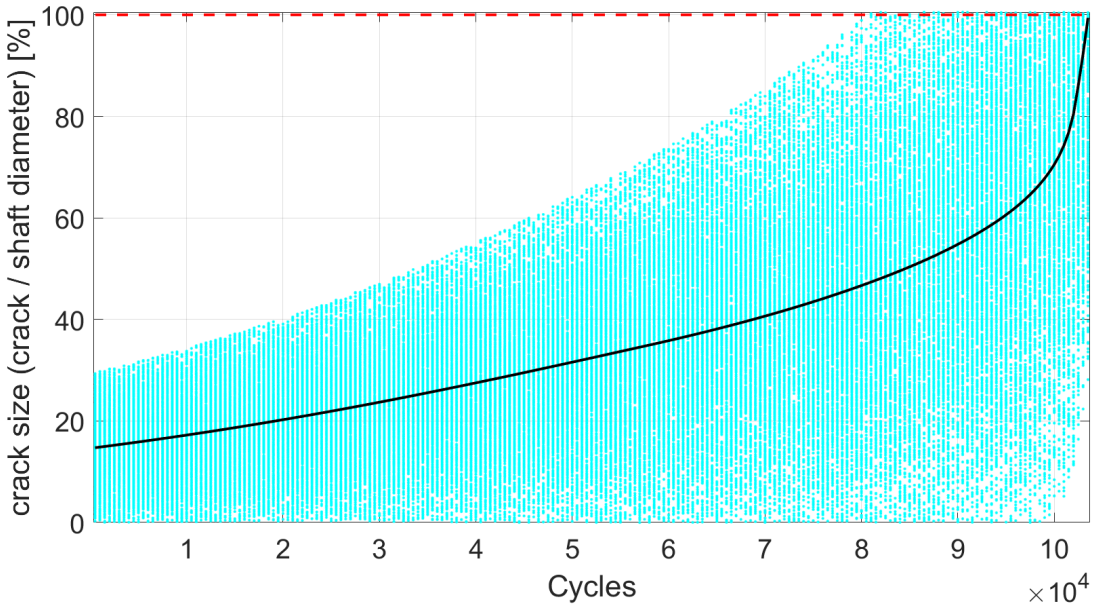

Figure 5: Plot of crack propagation with increasing number of cycles for the rotating shaft.

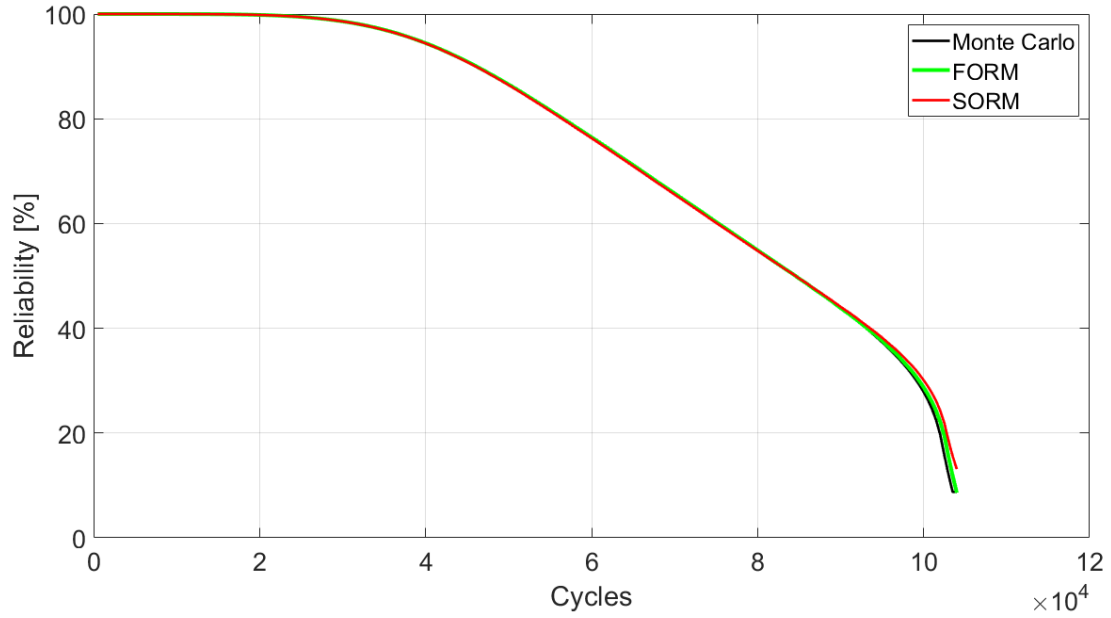

Figure 6: plot of reliability variation with increasing number of cycles for the rotating shaft.

making predictions at different failure levels with a high performance;

- Observation of the BNN model built allowed the evaluation of the epistemic uncertainty of the predictions, which ensures more information about the failure data of equipment, thus assisting in the process of monitoring the rotating machine condition and crack propagation using Paris Law and assessing Reliability with FORM and SORM;

Finally, we state that BNN is a powerful tool for assessing deep learning models. The combination of BNN with Paris Law, and FORM and SORM develops an intuitive framework supporting data generation for failure propagation in cases of equipment reliability assessment and remaining useful life estimation.

5. ACKNOWLEDGEMENTS

The authors acknowledge the financial support given by Brazilian Coordination for the Improvement of Higher Education Personnel (CAPES) and the Sao Paulo Research Foundation (FAPESP) [grant number #2019/00974-1].

6. REFERENCES

Alves, D.S., Daniel, G.B., de Castro, H.F., Machado, T.H., Cavalca, K.L., Gecgel, O., Dias, J.P. and Ekwaro-Osire, S., 2020. "Uncertainty quantification in deep convolutional neural network diagnostics of journal bearings with ovalization fault". *Mechanism and Machine Theory*, Vol. 149, p. 103835. ISSN 0094-114X. doi:https://doi.org/10.1016/j.mechmachtheory.2020.103835. URL `https://www.sciencedirect.com/science/article/pii/S0094114X20300562`.

Barbosa, M. and Rade, D., 2022. "Kriging/form reliability analysis of rotor-bearing systems". *Journal of Vibration Engineering & Technologies*, Vol. 10, No. 6, pp. 2179–2201.

Blundell, C., Cornebise, J., Kavukcuoglu, K. and Wierstra, D., 2015. "Weight uncertainty in neural network". In *International Conference on Machine Learning*. PMLR, pp. 1613–1622.

de Moraes, M., Dias, J.P. and de Castro, H.F., 2021. "Condition monitoring of ball bearings using bayesian neural networks". In *Proceedings of the XLII Ibero-Latin-American Congress on Computational Methods in Engineering and III Pan-American Congress on Computational Mechanics, ABMEC-IACM*. Rio de Janeiro, pp. 1–7.

Du, Y., Zhou, S., Jing, X., Peng, Y., Wu, H. and Kwok, N., 2020. "Damage detection techniques for wind turbine blades: A review". *Mechanical Systems and Signal Processing*, Vol. 141, p. 106445.

Endeshaw, H.B., Ekwaro-Osire, S., Alemayehu, F.M. and Dias, J.P., 2017. "Evaluation of fatigue crack propagation of gears considering uncertainties in loading and material properties". *Sustainability*, Vol. 9, No. 12, p. 2200.

Garoli, G.Y. and de Castro, H.F., 2020. "Generalized polynomial chaos expansion applied to uncertainties quantification in rotating machinery fault analysis". *Journal of the Brazilian Society of Mechanical Sciences and Engineering*, Vol. 42, No. 11, pp. 1–15.

Iliyas Ahmad, M., Yusof, Y., Daud, M.E., Latiff, K., Abdul Kadir, A.Z. and Saif, Y., 2020. "Machine monitoring system: a decade in review". *The International Journal of Advanced Manufacturing Technology*, Vol. 108, No. 11, pp. 3645–3659.

Kang, R., Zhang, Q., Zeng, Z., Zio, E. and Li, X., 2016. "Measuring reliability under epistemic uncertainty: Review on non-probabilistic reliability metrics". *Chinese Journal of Aeronautics*, Vol. 29, No. 3, pp. 571–579.

Kitai, M., Kobayashi, T., Fujiwara, H., Tani, R., Numao, M. and Fukui, K.I., 2021. "A framework for predicting remaining useful life curve of rolling bearings under defect progression based on neural network and bayesian method". *IEEE Access*, Vol. 9, pp. 62642–62652. doi:10.1109/ACCESS.2021.3073945.

Liu, R., Yang, B., Zio, E. and Chen, X., 2018. "Artificial intelligence for fault diagnosis of rotating machinery: A review". *Mechanical Systems and Signal Processing*, Vol. 108, pp. 33–47.

Ma, S.B., Kim, S. and Kim, J.H., 2020. "Optimization design of a two-vane pump for wastewater treatment using machine-learning-based surrogate modeling". *Processes*, Vol. 8, No. 9, p. 1170.

Nannapaneni, S. and Mahadevan, S., 2016. "Reliability analysis under epistemic uncertainty". *Reliability Engineering & System Safety*, Vol. 155, pp. 9–20.

Oliveira, J.C.S., 2013. "Análise de indicadores de qualidade e produtividade da manutenção nas indústrias brasileiras". *Revista Gestão da Produção Operações e Sistemas*, Vol. 9, No. 3, p. 53.

Paris, P. and Erdogan, F., 1963. "A critical analysis of crack propagation laws".

Peng, W., Ye, Z.S. and Chen, N., 2020. "Bayesian deep-learning-based health prognostics toward prognostics uncertainty". *IEEE Transactions on Industrial Electronics*, Vol. 67, No. 3, pp. 2283–2293. doi:10.1109/TIE.2019.2907440.

San Martin, G., López Droguett, E., Meruane, V. and das Chagas Moura, M., 2019. "Deep variational auto-encoders: A promising tool for dimensionality reduction and ball bearing elements fault diagnosis". *Structural Health Monitoring*, Vol. 18, No. 4, pp. 1092–1128.

Sun, J., Wang, L., Li, J., Li, F., Li, J. and Lu, H., 2021. "Online oil debris monitoring of rotating machinery: A detailed review of more than three decades". *Mechanical Systems and Signal Processing*, Vol. 149, p. 107341.

Vega, M.A. and Todd, M.D., 2020. "A variational bayesian neural network for structural health monitoring and cost-informed decision-making in miter gates". *Structural Health Monitoring*, Vol. 00, pp. 1–15.

Wang, H., Bai, X. and Tan, J., 2020. "Uncertainty quantification of bearing remaining useful life based on convolutional neural network". In *2020 IEEE Symposium Series on Computational Intelligence (SSCI)*. pp. 2893–2900. doi:10.1109/SSCI47803.2020.9308463.

Wang, R., Chen, H. and Guan, C., 2021. "A bayesian inference-based approach for performance prognostics towards uncertainty quantification and its applications on the marine diesel engine". *ISA transactions*, Vol. 118, pp. 159–173.

7. RESPONSIBILITY NOTICE

The authors are solely responsible for the printed material included in this paper.